Available online at www.sciencedirect.com
SCIENCE DIRECT®
Journal of Sound and Vibration 265 (2003) 359–386
JOURNAL OF SOUND AND VIBRATION
www.elsevier.com/locate/jsvi

Self-sustained oscillations in a closed side branch system

S. Dequand[a], S.J. Hulshoff[b], A. Hirschberg[a,*]

[a] *Technische Universiteit Eindhoven, Postbus 513, 5600 MB Eindhoven, Netherlands*
[b] *Faculty of Aerospace Engineering, Technische Universiteit Delft, Kluyverweg 1, 2629 HS Delft, Netherlands*

Received 10 December 2001; accepted 10 July 2002

Abstract

Self-sustained oscillations of the flow in a closed side branch system due to a coupling of vortex shedding with acoustical resonances are considered. The configuration consists of two closed side branches of same length placed opposite to each other along a main pipe. This is called a cross-junction. Numerical simulations, based on the Euler equations for two-dimensional inviscid and compressible flows, are performed. As the radiation into the main pipe is negligible at the resonance frequency, this acoustically closed system is a good test-case of such Euler numerical calculations. The numerical results are compared to acoustical measurements and flow visualization obtained in a previous study. Depending on the flow conditions, the predicted pulsation amplitudes are about 30–40% higher than the measured amplitudes. This is partially due to the absence of visco-thermal dissipation in the numerical model but also to the effect of wall vibrations in experiments. A simple analytical model is proposed for the prediction of the pulsation amplitudes. This model is based on Nelson's representation of the shear layer as a row of discrete vortices convected at constant velocity from the upstream edge towards the downstream edge. When the downstream edge is sharp, this results in a spurious interaction between the singularity of the vortices and of the edge flow. This artefact is partially compensated by suppressing the singularity of the acoustical flow at the edge, or when a junction with rounded edges, as found in engineering practice, is considered. In spite of its crudeness, the analytical model provides a fair prediction (within 30%) which makes it useful for engineering applications.

1. Introduction

Self-sustained oscillations can appear when a flow is grazing along deep cavities. The flow separation induces the formation of a shear layer separating the main flow from the stagnant fluid

*Corresponding author.
E-mail address: a.hirschberg@tue.nl (A. Hirschberg).

0022-460X/03/$ - see front matter © 2002 Elsevier Science Ltd. All rights reserved.
doi:10.1016/S0022-460X(02)01458-X

in the cavity. This shear layer is unstable. The coupling between resonant acoustic standing waves in the cavity and instabilities of the shear layer results in self-sustained oscillations.

The phenomenon of self-sustained oscillations is due to an acoustic feedback loop in which the shear layer can be represented as an amplifier (Fig. 1). The acoustic resonant modes of the cavity determine the oscillation frequency.

Strong resonances can be observed in pipe systems with closed side branches. The case in which the side branches have the same diameter as the main pipe is considered. A closed side branch of length L along a main pipe is an almost perfect reflector at critical resonance frequencies $f_m = mc/(4L)$ (where $m = 2n + 1$ with $n = 0, 1, 2, \ldots$ and c is the speed of sound), but it is not a resonator on its own [1–3].

A closed resonator can be formed by two such resonant closed side branches placed at a distance $L_n \approx (c/2f)n$ from each other along the main pipe (f is the resonance frequency and $n = 0, 1, 2, \ldots$) [1,4]. Fig. 2 shows two examples of such resonators.

Consider the case in which the pipes have the same length $L = c/4f$ and are placed opposite to each other ($n = 0$, Fig. 2b). This configuration is called a cross-junction and is studied in this paper.

In case of deep cavities, Elder [5] and Howe [6] proposed a model based on a linear response of the shear layer. The oscillation amplitude of the shear layer increases exponentially with the distance from the upstream edge. This model is limited to very low amplitudes ($u'/U_0 \leqslant 10^{-3}$, where u' is the amplitude of the acoustical component of the velocity and U_0 is the mean flow velocity). This is called the low-amplitude regime.

For larger amplitudes, the shear layer breaks down into discrete vortices [7].

For moderate amplitudes ($10^{-2} \leqslant u'/U_0 \leqslant 10^{-1}$), while the formation of discrete vortices is triggered by the acoustic velocity field, the amount of vorticity shed remains, however, independent of the amplitude of the acoustic field [1]. It is controlled by the mean flow. It is essentially equal to the amount of vorticity shed in the steady flow case when there are no oscillations. The empirical model of Nelson et al. [7] for a Helmholtz resonator assumes that the vorticity is concentrated into line vortices convected at a constant velocity $U_\Gamma = 0.4U_0$ along a line joining the upstream to the downstream edge. Earlier applications of the model to a junction with sharp edges by Bruggeman et al. [1] and Howe [6], overestimate the pulsation amplitudes by a factor of three or more. This appears to be due to the interaction of a singularity in the vorticity field, the point vortex, with a singularity in the acoustic field at the sharp downstream edge. In

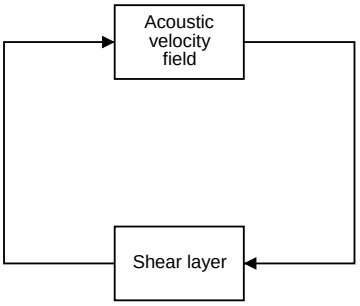

Fig. 1. Acoustic feedback loop characterizing the phenomenon of self-sustained oscillations.

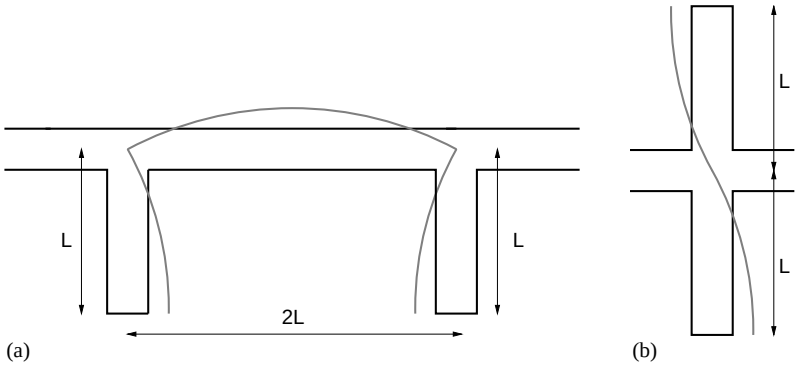

Fig. 2. Two reflectors placed at a distance $L_n = nc/2f$ from each other (closed resonators): (a) case $n = 1$, (b) case $n = 0$. The resonant acoustic mode in pressure perturbation is shown.

practice, this strong interaction does not occur because the vorticity is not concentrated into a point [1] and because the vortex path deviates from the straight line assumed in Nelson's model [6]. The fact that the vortex does not always hit the downstream edge is very clearly seen in the flow visualizations and vortex-blob numerical simulations of Kriesels et al. [3] which are used as test-case of our own numerical and analytical models (Section 5.2). It will be shown that when the singularity of the acoustical flow at the sharp edge is removed, the prediction of the model is improved. Furthermore, the effect of the sharpness of the edges is studied by considering results obtained for a junction with rounded edges [1–3]. As pipe junctions have rounded edges in most engineering applications, this is quite relevant.

In this paper, the proposed analytical model is based on the Nelson's model but in which the singularity of the acoustical flow at the downstream edge is suppressed (Section 3). This allows better prediction of the pulsation amplitude. In Section 2, a summary of experimental data obtained by Peters [2] and Kriesels et al. [3] is provided. Experimental data are then compared to original numerical simulations based on the Euler equations for two-dimensional compressible flows (Section 4). As the Euler code used here has been described in some details in other papers [8–10], the focus will be on the description of the analytical model. From earlier work on wall cavities [10,11], it appears that the numerical results depend crucially on the acoustical boundary conditions outside the cavity. The problem is due to the difficulty in converting 3-D acoustical boundary conditions outside the cavity into a 2-D numerical code. The present case of a cross-junction has the great advantage to remain a 2-D problem in the entire flow. Furthermore, the self-sustained oscillations are not sensitive to the acoustical boundary conditions at the inflow and outflow planes in the main pipe. This provides an excellent test of the aero-acoustical performances of the Euler code over the bulk of the flow.

The results are also compared to numerical results obtained by using a point-vortex model assuming a locally two-dimensional incompressible potential flow model. This method is described in detail by Peters [2], Kriesels et al. [3] and Hofmans [12]. The point vortices are desingularized using the method proposed by Krasny [13]. This is called a vortex-blob method. Accurate calculations carried out by Hofmans [12] for a similar case (single side branch system)

appear to predict the pulsation amplitudes within 10% for $u'/U_0 < 0.1$. For $u'/U_0 = O(1)$, the model overestimates the pulsation level by 30%.

Using Howe's energy corollary (see Eq. (5)), this incompressible flow simulation provides a prediction of the acoustical power generated by the flow at the junction. By using an energy balance which includes visco-thermal losses and the effect of shock wave formation, one can predict the pulsation amplitude [3,12]. For moderate amplitudes, Kriesels et al. [16] propose a simplified approach based on the assumption that the sound power generated by the flow is proportional to the pulsation amplitude. This approach will be described more in detail in Section 2.3. Furthermore, the estimation given by Kriesels [3] of the effect of shock wave formation will be corrected as proposed by Hofmans [12].

2. Previous experimental and numerical studies

2.1. Experimental setup

A summary of the experimental results of Peters [2] and Kriesels et al. [3] is provided here, and they are compared to our theoretical models. Fig. 3 shows a scheme of the experimental setup. A complete description of the experimental setup can be found in Refs. [2,3]. The closed side branches and the main pipe have a square cross-section area of $H \times H = 60 \times 60$ mm^2. The pipes have aluminium walls with a thickness of 2 mm.

A drawback of the square pipe cross-section used in this set-up is that it makes the system rather sensitive to wall vibrations. Kriesels et al. [17] report maximum pulsation amplitudes $(u'/U_0)_{\max} = 1.2$ for the junction with rounded edges, while Peters [2] reports $(u'/U_0)_{\max} = 1.3$. This observed difference is partially due to the consolidation of the pipes by gluing steel plates of

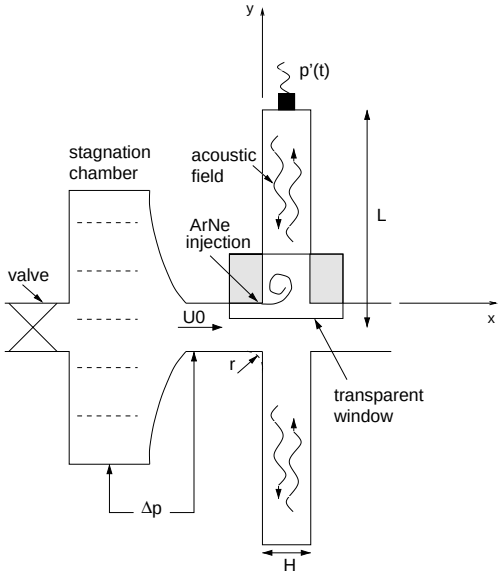

Fig. 3. Experimental setup (from Ref. [2]).

3 mm thickness on the outer walls of the closed side branches. Furthermore, experiments carried out at high pressures (10 bar) with circular steel pipes of 2.5 cm of diameter and a wall thickness of 5 mm, give a maximum of pulsation amplitude of $(u'/U_0)_{\max} = 1.4$ [15]. This confirms that the pulsation levels in the data presented by Kriesels et al. [3] may have been reduced by at least 15% due to wall vibrations.

The main flow is generated by a wind tunnel and passes through a settling chamber with square cross-section (with a width of 0.35 m). The air flows into the main pipe through a smooth contraction, placed one side branch width H upstream of the cross-junction. The magnitude of the velocity U_0 of the main flow is calculated from the pressure difference Δp measured across the contraction by means of a Betz water manometer (accuracy ± 1 Pa). The steady flow Bernoulli equation is used: $U_0 = \sqrt{2\Delta p/\rho}$ (with ρ being the density of air). The acoustical pressure amplitude p'_{exp} and the oscillation frequency f are measured at the end of one of the closed side branches by means of a piezo-electric microphone. The amplitude of the acoustic velocity field at the junction is then deduced by assuming that only plane waves propagate into the closed side branches: $u'(y) = p'_{exp}\sin(k_m y)/(\rho c)$ (with $k_m = m\pi/(2L)$ the wave number where $m = 2n + 1$, $n = 0, 1, 2, \ldots$). The length L of the closed side branches can be varied and is defined as the distance between the end of the closed side branch and the middle of the main pipe (Fig. 3). The effect of the deviation from the plane wave behaviour at the junction has been neglected. This deviation would involve an 'end-correction' of the order of one third of the pipe width H [16].

In the region where the vortices are formed, the side walls of the cross-junction are made up of glass windows. A Schlieren method is used to visualize the flow. A more detailed description of this method is given by Peters [2]. The necessary difference in refractive index is obtained by injecting a mixture of 50% Ar and 50% Ne, which has a density ρ and speed of sound c very close to that of air. In this way, the injection of this mixture does not affect the acoustical behaviour of the cross-junction. A nanolite light source generates a light pulse each time the acoustic pressure at the end of a closed side branch exceeds a certain value. A delay between the trigger signal and the nanolite pulse is introduced in order to visualize the flow at a different moment of the oscillation period $T = 1/f$. Only the vortex formation in the upper shear layer was visualized. It is identical to the vortex formation in the lower shear layer, but with a phase shift of half an oscillation period.

The experiments were carried out by Peters [2] on two different cross-junctions. The first cross-junction had sharp edges (Fig. 4a) and the second had rounded edges with a radius of curvature $r = 0.2H$ where $H = 60$ mm is the width of the side branch (Fig. 4b).

2.2. Acoustic and hydrodynamic modes

The different acoustic modes in a cross-junction with circular pipes have been observed experimentally by Peters [2] and Kriesels et al. [3]. These results are used to explain the different oscillation modes of the system. Fig. 5a gives an example of the results obtained for the amplitude of the acoustical pressure $p'(t)$ measured at the top of one closed side branch of the cross-junction and the corresponding frequency f in terms of the main flow velocity U_0. The graph of frequency versus the main flow velocity U_0 shows the different resonant acoustic modes $f_m = mc/(4L)$ in a cross-junction. They correspond to closed side branches with a length $L = m\lambda/4$ where $m = 2n + 1$ ($n = 0, 1, 2, \ldots$) (Fig. 5b). Only the odd modes are resonant because they have a pressure

node at the junction. The even modes ($m = 2n$, $n = 0, 1, 2, \ldots$), which have a pressure anti-node at the junction, radiate strongly into the main pipe.

As can be seen in Fig. 5a, pulsations occur at a certain frequency (acoustic mode) within limited ranges of flow velocities which correspond to so-called hydrodynamic modes. In Fig. 5a, the first

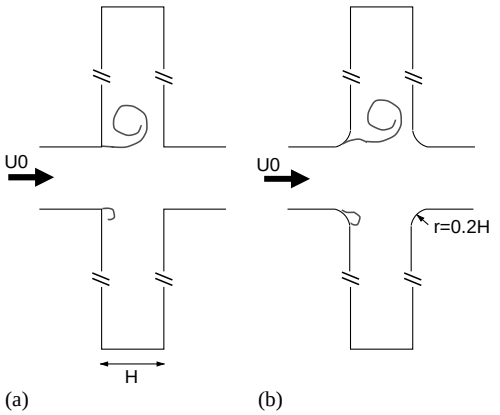

Fig. 4. Configurations studied. (a) Cross-junction with sharp edges; (b) cross-junction with rounded edges ($r/H = 0.2$).

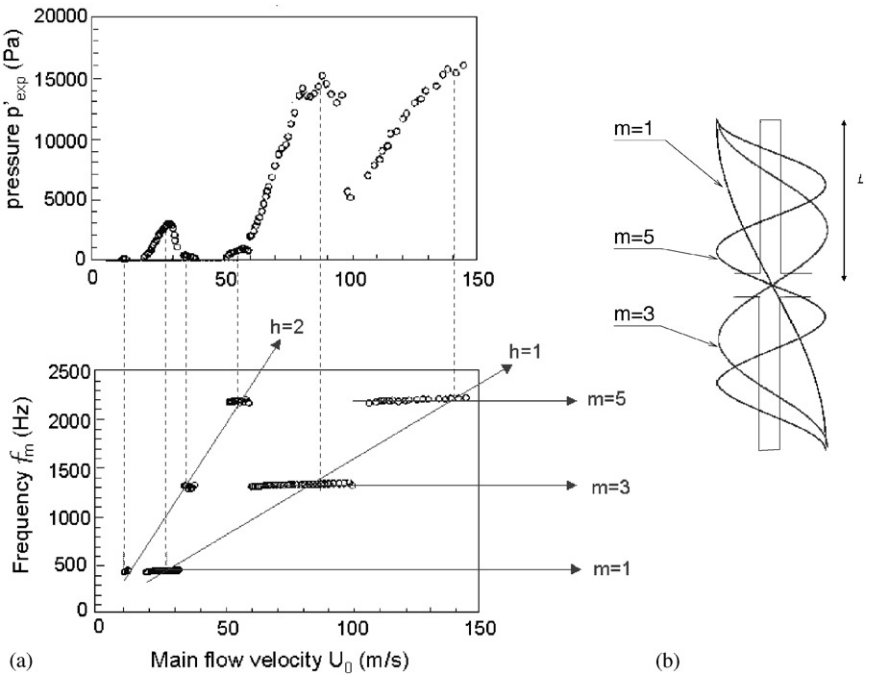

Fig. 5. Acoustical measurements of a cross-junction with circular pipes obtained by Kriesels [3]: (a) acoustical pressure at the top of a closed side branch and frequency in terms of the main flow velocity U_0, (b) resonant acoustic modes in pressure perturbations in a cross-junction.

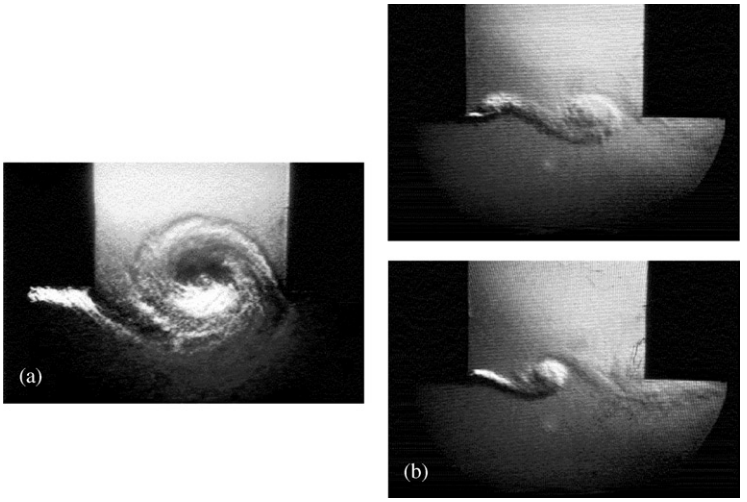

Fig. 6. Flow visualization in a cross-junction [2]: (a) first hydrodynamic mode ($h = 1$), (b) second hydrodynamic mode ($h = 2$), two successive pictures of the vortices.

hydrodynamic mode is indicated by the line $h = 1$, the second by the line $h = 2$. In the first hydrodynamic mode ($h = 1$), only one vortex per oscillation period T is shed (Fig. 6a) and the acoustical pressure $p'(t)$ at the end of the closed side branches presents different maxima at critical Strouhal numbers $S_r = fH/U_0$. In the second hydrodynamic mode ($h = 2$), the time needed by a vortex to travel through the junction is about two oscillation periods. This implies that two vortices are present at the same time in the opening of the side branch. This is shown by the flow visualization of Fig. 6b.

2.3. Vortex-blob method

In the earlier work of Peters [2], Kriesels et al. [3,14] and Hofmans [12], the amplitude of the pulsations was predicted by means of an energy balance, which is also used in our analytical modelling. In the vortex-blob calculations, the acoustical velocity u' at the junction is imposed as a boundary condition. At first, the acoustical power $\langle \mathscr{P}_{source} \rangle$ generated by the vortical flow is calculated, for a given Strouhal number, as a function of the amplitude of the acoustical velocity field ($u'/U_0 = O(10^{-1})$). This acoustical power is then equalized to the energy losses due to visco-thermal dissipation in the closed side branches and to radiation of even modes (Section 2.2). The loss terms will be discussed in details in Section 3.2. The aero-acoustical source power can be calculated by carrying out, at a fixed Strouhal number, vortex-blob calculations of the flow at different amplitudes u'/U_0. This procedure was used by Peters [2], Kriesels et al. [3] and Hofmans [12] (Section 1).

The flow calculated on the basis of the measured pulsation amplitudes $(u'/U_0)_{exp}$ will be compared with experimental flow visualization [2,3] and with our own Euler computations. These results will be referred to in Section 4 as Peters' blob method. The use of such calculations in an energy balance involves a significant computational power. Therefore for engineering

applications, a simplified model based on the concept of moderate amplitudes $u'/U_0 = O(10^{-1})$ is considered [1]. For such moderate amplitudes $u'/U_0 = O(10^{-1})$, the power generated by the flow is assumed to be proportional to the pulsation amplitude. As can be seen later from Howe's energy corollary (Eq. (5)), this implies that $(\boldsymbol{\omega} \times \boldsymbol{v})$ is independent of the amplitude. Detailed numerical calculations on a single closed side branch system showed that the acoustical power $\langle \mathscr{P}_{source} \rangle$ is approximately (within 20%) linearly dependent on u'/U_0 for $u'/U_0 < 0.3$ [14]. The dimensionless source power $\langle \mathscr{P}_{source} \rangle / (\rho_0 U_0^2 u' H^2)$ is calculated by Kriesels for the cross-junction and is compared for different radii of curvature R of the junction edges [17] to our new analytical results in Section 3.2.5. These data are used further in Section 5 and are referred to as Kriesels' vortex-blob method.

3. Theory

3.1. Vortex-sound theory [18,19]

Following the analogy of Howe [19], the acoustical velocity $\boldsymbol{u}'$ is defined as the unsteady irrotational part of the velocity field $\boldsymbol{v}$:

$$\boldsymbol{v} = \boldsymbol{\nabla}(\phi_0 + \phi_{ac}(t)) + \boldsymbol{\nabla} \times \boldsymbol{\Psi}, \tag{1}$$

$$\boldsymbol{u}' = \boldsymbol{\nabla}\phi_{ac}(t), \tag{2}$$

where $\phi = \phi_0 + \phi_{ac}(t)$ is the scalar potential and $\boldsymbol{\Psi}$ is the vector stream function. The ambiguity of this definition is removed by using the boundary conditions of the problem. In the far field, the acoustical field corresponds to plane waves and has a zero velocity at the closed ends of the side branches.

If friction and heat transfer are neglected, a homentropic flow satisfies Crocco's form of the Euler equation

$$\frac{\partial \boldsymbol{v}}{\partial t} + \boldsymbol{\nabla} B = -\boldsymbol{\omega} \times \boldsymbol{v}, \tag{3}$$

where B is the total enthalpy defined by $B = i + |\boldsymbol{v}|^2/2$ (with $i = e + p/\rho$ the specific enthalpy) and the vorticity $\boldsymbol{\omega}$ is defined by $\boldsymbol{\omega} = \boldsymbol{\nabla} \times \boldsymbol{v}$.

Neglecting convective effects on the wave propagation ($M_0 = |\boldsymbol{u}_0|/c_0 \ll 1$) and assuming a compact source region (small compared to the wavelength), the wave equation is

$$\frac{1}{c_0^2}\frac{\partial^2 B}{\partial t^2} - \nabla^2 B = \boldsymbol{\nabla} \cdot (\boldsymbol{\omega} \times \boldsymbol{v}). \tag{4}$$

Hence, the Coriolis force density $\boldsymbol{f}_c = -\rho(\boldsymbol{\omega} \times \boldsymbol{v})$ is identified as the dominant source of sound in such flows.

This equation should at least provide an excellent approximation in the closed side branches where $U_0 = 0$.

With this level of approximation (low Mach number), the time average of the acoustic power $\mathscr{P}_{source}$ generated by the flow for periodic oscillations is given by

$$\langle \mathscr{P}_{source} \rangle = \left\langle -\rho_0 \int_V (\boldsymbol{\omega} \times \boldsymbol{v}) \cdot \boldsymbol{u}' \, \mathrm{d}V \right\rangle, \tag{5}$$

where $\langle\ \rangle$ denotes the time averaging over one period of oscillation [19].

3.2. Single-mode model

3.2.1. Simplified acoustical model

The cross-junction configuration forms a closed resonator which behaves as a forced linear acoustical system. If a single acoustical mode is assumed to be dominant, the acoustical displacement $\xi(t)$ in the source region ($y = 0$) is described by

$$M_a \frac{\mathrm{d}^2\xi}{\mathrm{d}t^2} + R\frac{\mathrm{d}\xi}{\mathrm{d}t} + K\xi(t) = \mathscr{F}(t), \tag{6}$$

where M_a represents the effective acoustical mass, R the damping, K the spring constant of the system and $\mathscr{F}(t)$ corresponds to the external forces which act on the system. These forces $\mathscr{F}(t)$ consist of the sum of an aeroacoustic source term due to vortices and radiation loss terms due to non-linear wave propagation. The aeroacoustic source term can be either determined by using the model of Nelson et al. [7] (Section 3.2.3) or the blob method [3,14]. The radiation loss term corresponds to transfer of energy from the fundamental oscillation mode to higher modes as a result of losses due to wave steepening (Section 3.2.2).

Determination of the effective acoustical mass M_a: The mass M_a is deduced by calculating the kinetic energy E_c of the system:

$$E_c = \frac{1}{2} M_a \left(\frac{\mathrm{d}\xi}{\mathrm{d}t}\right)^2 = H^2 \int_{-L}^{+L} \frac{1}{2}\rho_0 u'^2 \, \mathrm{d}y, \tag{7}$$

where u' is the local acoustical velocity amplitude, H and L are the width and the length of the side branches, respectively.

By assuming harmonic plane waves in the closed side branches, the acoustical pressure p', for the first acoustical mode $m = 1$, is

$$p'(y,t) = \hat{p}\cos(\omega t)\sin\left(\frac{\pi y}{2L}\right). \tag{8}$$

The linearized momentum conservation equation

$$\rho_0 \frac{\partial u'}{\partial t} = -\frac{\partial p'}{\partial y}, \tag{9}$$

then yields

$$u'(y,t) = \left(\frac{\mathrm{d}\xi}{\mathrm{d}t}\right)\cos\left(\frac{\pi y}{2L}\right). \tag{10}$$

So that, neglecting the effect of the deviation of the two-dimensional flow at the junction from the one-dimensional approximation (Eq. (10)),

$$M_a = \rho_0 H^2 L. \tag{11}$$

Determination of the spring constant K: The spring constant K is related to the resonance pulsation $\omega_0 = 2\pi f_0$ of the system by:

$$K = \omega_0^2 M_a, \tag{12}$$

where $f_0 \approx c_0/(4L)$. This level of accuracy in the prediction of f_0 is reasonable in view of other approximations in the model.

Determination of the damping coefficient R: The damping coefficient R is related to the quality factor $Q_f = \omega_0/\Delta\omega_{3dB}$ of the system

$$R = \frac{\omega_0 M_a}{Q_f}. \tag{13}$$

where $\Delta\omega_{3dB}$ is the width of the resonance peak at an amplitude which is a factor $\sqrt{2}$ lower than the maximum amplitude.

The main source of acoustic losses in a cross-junction is the wave attenuation in the closed side branches due to viscous dissipation and thermal conduction in the wall boundary layers. When acoustical plane waves are travelling through a stagnant uniform fluid in a pipe (of cross-section area A and perimeter L_p), their amplitude is decreasing with the distance x by an exponential factor $e^{-\alpha x}$ where α is the damping coefficient. When the visco-thermal boundary layers are thin compared to the pipe cross-section, Kirchhoff's result [20] can be used:

$$\alpha = \frac{L_p}{2A}\sqrt{\frac{v}{\pi f}}\left(1 + \frac{(\gamma - 1)}{\sqrt{Pr}}\right). \tag{14}$$

This damping coefficient α is related to the quality factor Q_f of the resonator formed by the two closed side branches. In the cross-junction, when the closed side branches have the same length L, a plane wave travelling along these closed side branches will cover a distance of $4L$ in one oscillation period T. For free oscillations, the attenuation of the plane-wave amplitudes in one oscillation period is then

$$\frac{p(T)}{p(0)} = e^{-4\alpha L} = e^{-\pi/Q_f}, \tag{15}$$

by definition of the quality factor Q_f which implies that $Q_f = \pi/(4\alpha L)$ and

$$R = 8 f_0 \rho_0 H^2 L^2 \alpha. \tag{16}$$

The visco-thermal acoustic losses are given by

$$\langle \mathscr{P}_{vth} \rangle = \left\langle R\left(\frac{d\xi}{dt}\right)^2 \right\rangle. \tag{17}$$

3.2.2. Non-linear radiation losses due to wave steepening

For high-amplitude oscillations, additional losses are found as a result of non-linear wave steepening. This deformation of the wave implies that higher harmonics are formed due to non-linearity. As discussed earlier, the even harmonics have a pressure anti-node at the junction with the main pipe and are therefore very efficiently radiated into the main pipe. Following here the analysis of Hofmans [12], these radiation losses depend on the ratio $\sigma = y/y_s$ where y is the distance travelled by the wave and y_s is the shock wave formation distance. For a sinusoidal signal $p(0,t) = \hat{p_0} \sin \omega t$, σ is given by

$$\sigma = \frac{y}{y_s} = \frac{\gamma + 1}{2\rho c^2} ky\hat{p_0} \tag{18}$$

with $\gamma = 1.4$ the ratio of specific heats, and $k = \omega/c$ the wave number. For $\sigma < 1$, the harmonics are given by the Fubini solution [21]

$$p_n(y,t) = \hat{p_0} \frac{2}{n\sigma} \mathrm{J}_n(n\sigma) \sin[n\omega(t - y/c)]. \tag{19}$$

The amplitude of the first four harmonics can be approximated (for small σ) by

$$\begin{aligned} \hat{p}_1 &= \hat{p_0}\left(1 - \frac{\sigma^2}{8}\right), \\ \hat{p}_2 &= \hat{p_0}\frac{\sigma}{2}, \\ \hat{p}_3 &= \hat{p_0}\frac{3\sigma^2}{8}, \\ \hat{p}_4 &= \hat{p_0}\frac{\sigma^3}{3}. \end{aligned} \tag{20}$$

For small values of σ, the main non-linear losses are due to the radiation losses of the second harmonic (and other even harmonics). The radiated power is

$$\langle \mathscr{P}_{rad} \rangle = \frac{\hat{p}_2^2 H^2}{\rho c}. \tag{21}$$

In our case,

$$\begin{aligned} ky &= \pi, \\ \hat{p_0} &= \hat{p}/2. \end{aligned}$$

By assuming that the acoustical displacement is harmonic ($\xi(t) = -\hat{\xi} \cos \omega t$), then $\hat{p} = \hat{\xi}\omega\rho c$. Finally, the radiated power becomes

$$\langle \mathscr{P}_{rad} \rangle = \frac{(\hat{\xi}\omega)^4 \rho_0 (\gamma + 1)^2 \pi^2 H^2}{2^8 c}. \tag{22}$$

These radiation losses can also be expressed in terms of a non-linear force

$$\mathscr{F}_{rad} = -\frac{8\mathscr{P}_{rad}}{3(\hat{\xi}\omega)^4}\left(\frac{\mathrm{d}\xi}{\mathrm{d}t}\right)^3. \tag{23}$$

This simplified model fails when a shock wave is formed ($L/y_s > 1$). This appears to be the case when the configuration with rounded edges is used (Fig. 4b). Peters obtained Schlieren pictures of this shock. The numerical simulations presented further will allow this effect to be taken into account and to verify its impact on the pulsation amplitudes.

3.2.3. Nelson's flow model

Nelson et al. [7] proposed a model in which the vorticity of the shear layer is concentrated into point vortices convected at a constant velocity ($U_\Gamma \approx 0.4U_0, 0, 0$) (empirical value from Bruggeman et al. [1] where U_0 is the main flow velocity). In this model, it is assumed that the vortices travel along a straight line from the upstream to the downstream edge.

In the absence of pulsations, the shear layer is a straight line. The circulation $\Delta\Gamma$ of a length Δx of this shear layer is

$$\Delta\Gamma = \oint_{\mathscr{C}} \boldsymbol{v}.\mathrm{d}\boldsymbol{S} = U_0 \Delta x, \tag{24}$$

where $\mathscr{C}$ is the contour of length Δx enclosing the segment of the shear layer (Fig. 7). This is due to the fact that other parts in the contour $\mathscr{C}$ do not contribute to the circulation because either $\boldsymbol{v} = 0$ (in the side branch) or $\boldsymbol{v}$ is perpendicular to the contour.

The rate of vorticity shed at the upstream edge is then

$$\frac{\mathrm{d}\Gamma}{\mathrm{d}t} = \left(\frac{\Delta\Gamma}{\Delta x}\right)\frac{\mathrm{d}x}{\mathrm{d}t} = U_0 U_c, \tag{25}$$

where the velocity U_c at which vortices are convected is an average between the main flow velocity U_0 and the zero velocity of the stagnant fluid in the closed side branches $U_c \approx 0.5U_0$. It is now assumed that at moderate pulsation amplitudes, the rate of vorticity shed ($\mathrm{d}\Gamma/\mathrm{d}t$) remains equal to its steady flow value. When the vorticity is concentrated into a line vortex travelling along the line $y_\Gamma = 0$ (Fig. 7), then for the vorticity field $\boldsymbol{\omega} = \boldsymbol{\nabla} \times \boldsymbol{v} = (0, 0, \omega_z)$

$$\omega_z = \Gamma(t)\delta(x - x_\Gamma(t))\delta(y), \tag{26}$$

where $x_\Gamma(t)$ is the position of a point vortex at time t

$$x_\Gamma(t) = U_\Gamma(t - t_n) \tag{27}$$

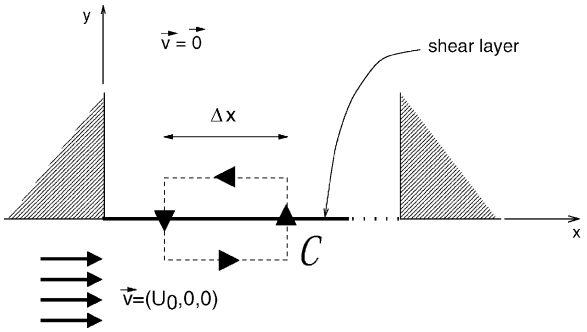

Fig. 7. Circulation in a segment of the shear layer enclosed by a contour $\mathscr{C}$.

with t_n being the time at which the nth vortex is shed. From empirical observations of Nelson et al. [7] and Bruggeman et al. [1], it appears that, for moderate amplitudes, a new vortex is shed each time the pressure in the closed side branch reaches a minimum. This can be taken as the time origin, so that, if a $(\cos \omega t)$-time dependence of the pressure is assumed:

$$t_n = (n-1)T \quad (n = 1, 2, \ldots). \tag{28}$$

The circulation Γ_n of the nth vortex depends on the time $T' = H/U_\Gamma$ needed by the vortex to travel through the junction and is defined as

$$\Gamma_n(t) = U_0 U_c g_n(t) \tag{29}$$

with

$$\begin{aligned} g_n(t) = {} & t[\mathscr{H}(t-t_n) - \mathscr{H}(t-T'-t_n)] && \text{if } T' \leqslant T, \\ g_n(t) = {} & t[\mathscr{H}(t-t_n) - \mathscr{H}(t-t_{n+1})] && \\ & + T[\mathscr{H}(t-t_{n+1}) - \mathscr{H}(t-t_n-T')] && \text{if } T' \geqslant T, \end{aligned} \tag{30}$$

where $\mathscr{H}(t)$ is the Heaviside function ($\mathscr{H}(t) = 0$ for $t<0$ and $\mathscr{H}(t) = 1$ for $t \geqslant 0$). The absolute value of the circulation $|\Gamma_n(t)|$ is drawn in Fig. 8.

If $T' \leqslant T$, only one vortex is present in the junction. This corresponds to the first hydrodynamic mode (Fig. 6a).

If $T' \geqslant T$, the first vortex has not yet reached the downstream edge while a second vortex is shed at the upstream edge of the junction. We have the second hydrodynamic mode (Fig. 6b).

The acoustic source power $\mathscr{P}_{source}$ produced by the vortices can be written in terms of the circulation $\Gamma_n(t)$. From Eq. (5):

$$\langle \mathscr{P}_{source} \rangle = \left\langle -\rho_0 \int_V (\boldsymbol{\omega} \times \boldsymbol{v}) \cdot \boldsymbol{u}' \, \mathrm{d}V \right\rangle = \langle -\rho_0 \Gamma_n(t) U_\Gamma H u'_y(x_\Gamma(t), y_\Gamma(t), t) \rangle, \tag{31}$$

where $\langle\ \rangle$ denotes the time averaging over one period of oscillation T and u'_y corresponds to the component in the y direction of the local acoustical velocity $\boldsymbol{u}'$ (as a result of the scalar product). Strictly speaking, an isolated vortex cannot have a time-dependent circulation without the

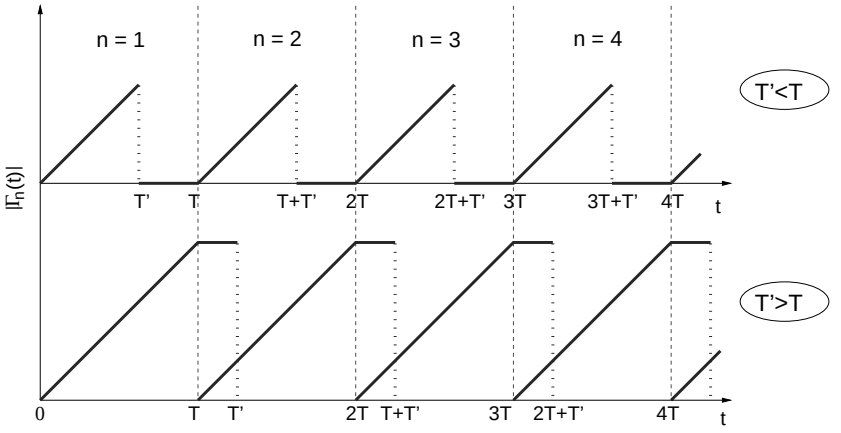

Fig. 8. Absolute value of the circulation $\Gamma_n(t)$ for $T' < T$ (upper graph) and $T' > T$ (lower graph).

presence of an external force. As our model assumes a time-dependent circulation $\Gamma(t)$, it does introduce a spurious force. However, by using Howe's analogy [19], the spurious force term is suppressed by simply ignoring it.

In the cross-junction, $\mathscr{P}_{source}$ is comparable to a source power associated with a source term Δp_{source}:

$$\langle \mathscr{P}_{source} \rangle = H^2 \langle \Delta p_{source} \cdot u'_y(x_\Gamma(t), y_\Gamma(t), t) \rangle. \tag{32}$$

In order to take into account the vortex shedding at both junction sides, Eq. (31) becomes

$$\langle \mathscr{P}_{source} \rangle = 2 \langle -\rho_0 \Gamma_n(t) U_\Gamma H u'_y(x_\Gamma(t), y_\Gamma(t), t) \rangle. \tag{33}$$

The acoustical source power $\mathscr{P}_{source}$ is related to the external forces $\mathscr{F}_{source}(t)$ which act on the system:

$$\langle \mathscr{P}_{source} \rangle = \left\langle (\mathscr{F}_{source})_y(t) \left(\frac{\mathrm{d}\xi}{\mathrm{d}t} \right) \right\rangle, \tag{34}$$

where $(\mathscr{F}_{source})_y(t)$ is the component in the y direction of the external forces $\mathscr{F}_{source}(t)$. It is related to a geometrical factor $\kappa_n(t)$ which takes into account the influence of the geometry:

$$(\mathscr{F}_{source})_y(t) = -\rho_0 \Gamma_n U_\Gamma H \kappa_n(t), \tag{35}$$

with $\kappa_n(t) = u'_y(x_\Gamma(t), y_\Gamma(t), t)/\frac{\mathrm{d}\xi}{\mathrm{d}t}$. $\kappa_n(t)$ is the ratio of the local vertical component of acoustical velocity to the average of this velocity along the vortex path.

3.2.4. *Effect of edge geometry*

Junction with rounded edges: As explained in the introduction, in most engineering applications, the junction has rounded edges. In that case, it is assumed that the acoustical flow has a one-dimensional behaviour (Fig. 9) and that the acoustical velocity in the junction has a uniform amplitude [22]. The geometrical parameter κ_n is then a constant. The value

$$\kappa_n(t) \approx \frac{1}{(1 + 2r/H)} \tag{36}$$

is used where r is the radius of curvature of the rounded edges and H is the width of the closed side branches. Eq. (36) is valid for $r/H = O(1)$.

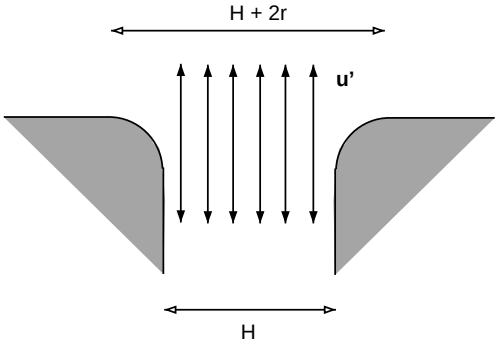

Fig. 9. Assumption of a uniform acoustical velocity in a junction with rounded edges.

Junction with sharp edges: In the case of a cross-junction with sharp edges ($r = 0$), the assumption of a uniform acoustic velocity is no longer valid because the acoustical velocity field is singular at the edges. At low frequencies, the acoustical flow at the junction is compact and can be considered as locally incompressible. As a locally incompressible acoustical flow at the junction is assumed, the geometric parameter $\kappa_n(t)$ can be calculated by means of a two-dimensional potential flow theory. This involves a conformal mapping of the geometry of the junction into a half plane.

In the Nelson et al. model [7], the vortex path is imposed and is a line joining the upstream to the downstream edge. It is expected that the interaction between the vortex and the downstream edge gives an exaggerated prediction of the response [1]. In order to avoid this interaction, the conformal mapping is applied to a modified geometry in which the downstream edge is replaced by a vertical wall (Fig. 10) is applied. In this way, the downstream singularity of the acoustical field is suppressed because its effect on the local flow at the vortex is ignored. An alternative to this arbitrary procedure would have been to assume a vortex path which passes at some distance from the edge as observed in the experiments (Section 5.2). Details of calculations of $\kappa_n(t)$ are given in the appendix.

Calculated source power: Fig. 11 shows the dimensionless acoustical source power $\langle \mathscr{P}_{source} \rangle / (\rho_0 U_0^2 H^2 \hat{\xi} \omega_0)$ calculated by means of our simple model as a function of the Strouhal number $S_r = fH/U_0$. The results are compared to the theoretical data obtained by Kriesels et al. [14] by means of the vortex-blob method for moderate amplitudes.

The acoustic power $\langle \mathscr{P}_{source} \rangle$ predicted by our simple model is a factor of three larger than the value predicted by means of the vortex-blob method by Kriesels et al. [14]. It can also be seen in Fig. 11 that the Strouhal number at which the source power is maximum matches for both models. The quality of the two models will be assessed further in Section 5 by comparison with experimental data and numerical results from the Euler computations.

3.2.5. *Prediction of the pulsation amplitude at the junction*

Method of averaging ($\omega \neq \omega_0$): The single-mode model proposed can predict the dimensionless pulsation amplitude $\chi = \hat{\xi}\omega/U_0$ and also the dimensionless frequency $\varepsilon = \omega/\omega_0$ in terms of the Strouhal number $S_r = \omega H/(2\pi U_0)$ based on the width H of the closed side branches. The model is based on the equation of motion (Eq. (6)) for the mean acoustical displacement ξ in the

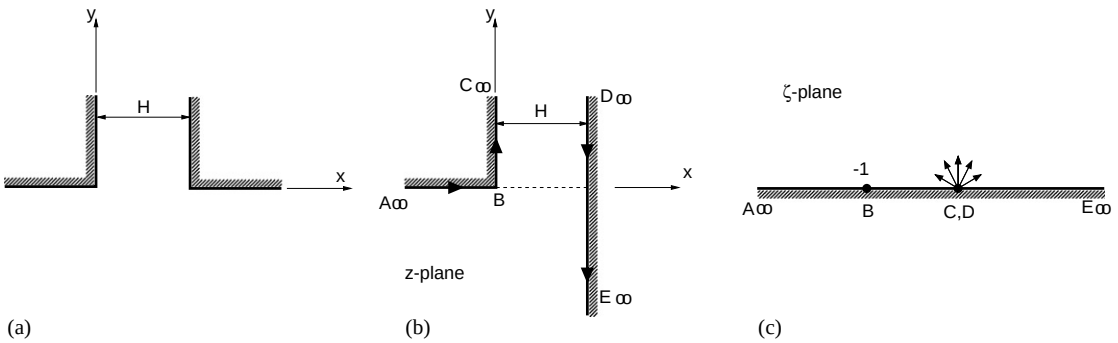

Fig. 10. (a) Actual geometry; (b) modified geometry chosen in order to suppress the singularity of the downstream edge (z-plane); (c) transformed plane by means of a conformal mapping (ζ-plane).

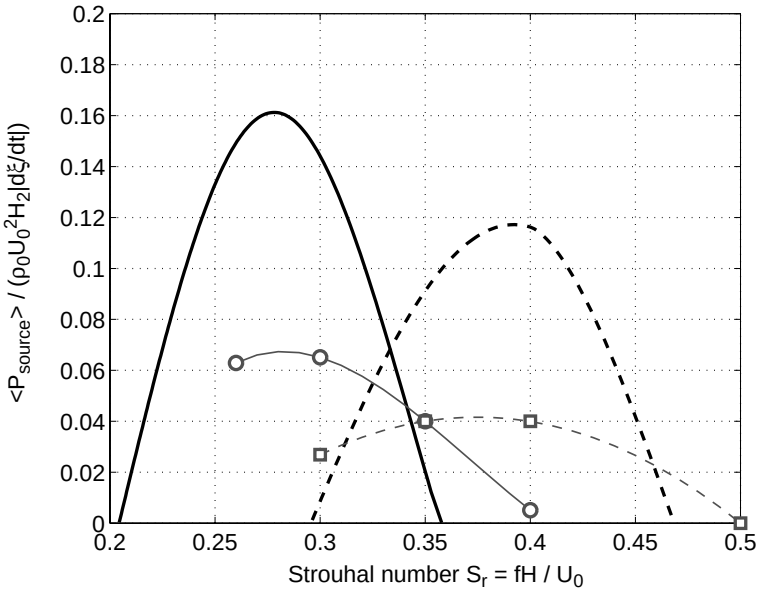

Fig. 11. Dimensionless acoustical source power $\langle \mathscr{P}_{source} \rangle / (\rho_0 U_0^2 H^2 \hat{\xi} \omega_0)$ as a function of the Strouhal number $S_r = fH/U_0$ (based on the pipe width H). Comparison of the results obtained by means of the energy balance calculated with the Nelson et al. model [7] (continuous and dashed lines) and with Kriesels' vortex-blob method for moderate amplitudes (open symbols, Ref. [3]). The results are shown for a cross-junction with rounded edges ($r/H = 0.2$) (——, ◦), and with sharp edges (– – – –, □).

cross-junction:

$$\frac{\mathrm{d}^2\xi}{\mathrm{d}t^2} + \frac{\omega}{Q_f}\frac{\mathrm{d}\xi}{\mathrm{d}t} + \omega^2\xi = \frac{\mathscr{F}_{source}}{M_a} + \frac{\mathscr{F}_{rad}}{M_a}, \tag{37}$$

where $\mathscr{F}_{source}$ and $\mathscr{F}_{rad}$ represent the forces related to the source power $\mathscr{P}_{source}$ and the radiated power $\mathscr{P}_{rad}$ (Eqs. (35) and(23)).

Assuming that the acoustic displacement is harmonic ($\xi(t) = -\hat{\xi}\cos\omega t$), a non-linear equation is obtained which relates the dimensionless frequency ω/ω_0 and the dimensionless pulsation amplitude $\hat{\xi}\omega/U_0$. The method of averaging is used. This consists of multiplying Eq. (37) by either $\cos\omega t$ or $\sin\omega t$ and integrating the two resulting equations over an oscillation period [23]. A system of two non-linear equations is obtained for two unknowns $\chi = \hat{\xi}\omega/U_0$ and $\varepsilon = \omega/\omega_0$. This set of equations is solved using Newton's method, initialized by means of the results of the energy balance.

Energy balance ($\omega = \omega_0$): The energy balance method is a simplified approach in which the deviation of the frequency f from the resonance frequency f_0 is assumed to be very small. Using the assumption $f = f_0$, the energy balance of the system is obtained. From Eqs. (17), (33) and (22), the energy balance of the system can be written by the balance of the sources and the losses:

$$\langle \mathscr{P}_{source} \rangle = \langle \mathscr{P}_{vth} \rangle + \langle \mathscr{P}_{rad} \rangle, \tag{38}$$

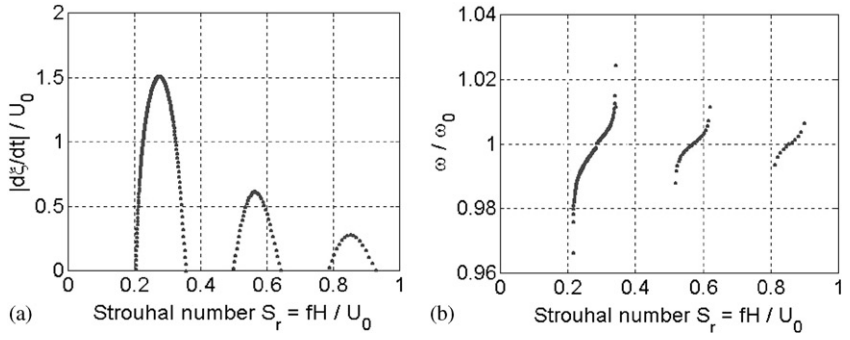

Fig. 12. Dimensionless amplitude $|\mathrm{d}\xi/\mathrm{d}t|/U_0$ (a) and dimensionless frequency ω/ω_0 (b) predicted by the single-mode model, as a function of the Strouhal number $S_r = fH/U_0$ (based on the pipe width H). The results are shown for a cross-junction with rounded edges ($r/H = 0.2$) with closed side branches of length $L = 0.61$ m.

$$-\frac{2}{T}\rho_0 U_\Gamma H \int_0^T \Gamma_n(t)\kappa_n(t)\left(\frac{\mathrm{d}\xi}{\mathrm{d}t}\right)\mathrm{d}t = \frac{R}{T}\int_0^T \left(\frac{\mathrm{d}\xi}{\mathrm{d}t}\right)^2 \mathrm{d}t + \frac{(\hat{\xi}\omega_0)^4\rho_0(\gamma+1)^2\pi^2H^2}{2^8 c}, \tag{39}$$

where $\kappa_n(t)$ has been introduced in the previous paragraph and where it has been assumed that $\omega = \omega_0$. From Eq. (39), the pulsation amplitude $\hat{\xi}\omega_0/U_0$ can be deduced. The energy balance appears to provide quite reasonable results in our case. The predicted amplitudes of both methods are almost identical because, in the particular case considered, the variation in frequency is small (Fig. 12).

4. Numerical computations

4.1. Approach

Numerical simulations have been performed for the cross-junctions (Fig. 4) using the Euler equations for two-dimensional inviscid and compressible flow [9]. The spatial discretization method is based on a second order cell-centred finite-volume method. For the time integration, a second order, low-storage, four-stage Runge–Kutta method was used with one evaluation of the artificial dissipation during the first stage. Results and tests of this code are presented in earlier papers [8,10].

4.2. Numerical parameters

4.2.1. Initial condition

Numerical simulations were initialized by specifying a pressure profile in the closed side branches. This pressure profile corresponds to a harmonic standing wave at the moment ($t = 0$) that the acoustical pressure at the closed side branch terminations is maximum and equal to the measured amplitude p'_{exp} of the pressure fluctuations: $p'(y, t = 0) = p'_{exp}\sin(2\pi f_0 y/c)$ (where f_0 is

the measured oscillation frequency). The initial velocity amplitude in the closed side branches was set to zero ($(u_x, u_y) = (0, 0)$), while the initially uniform velocity in the main pipe was set to the value of the experimental mean flow velocity ($(u_x, u_y) = (U_0, 0)$).

4.2.2. Boundary conditions

Boundary conditions are defined by specifying the state of halo cells surrounding the numerical domain. As proposed by Thompson [24,25], and Poinsot and Lele [26], this is done by using a local discretization of the compatibility relations.

The walls of the main pipe and the closed side branches were defined by imposing solid wall conditions (zero normal velocity component) along the corresponding boundaries of the numerical domain. An anechoic boundary condition was imposed on the outflow boundary (no acoustic wave reflection). A 'soft' constant-velocity condition was applied at the inflow boundary by specifying the strength of incoming acoustic waves to be proportional to the difference between the instantaneous velocity and the desired velocity, multiplied by a relaxation factor. In our computations, the value of this relaxation factor was fixed at 0.5. The boundary conditions imposed on the boundaries of the numerical domain are shown in Fig. 13.

4.2.3. Numerical domain

The numerical domain used for computations on a cross-junction with sharp edges is shown in Fig. 13. The numerical domain consists of structured grid blocks. The block just at the junction

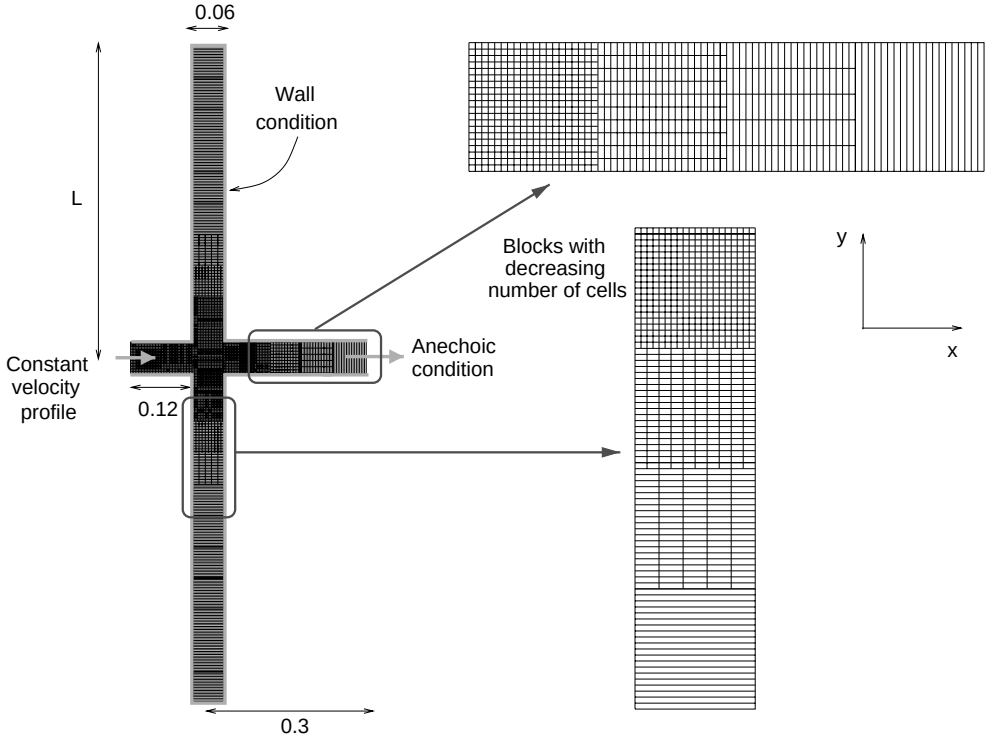

Fig. 13. Numerical domain used for Euler computations. Sketch of the boundary conditions imposed.

between the main pipe and the closed side branches contained 40 cells both in x and y directions. This region corresponds to the region where vortices are formed (source region). In the downstream part of the numerical domain (two diameters downstream of the closed side branches), the blocks in the main pipe had a gradually decreasing number of cells in the y direction. The coarse discretization in this 'buffer' region acted to reduce the vorticity leaving the numerical domain. In the closed side branches, the number of cells in the blocks was gradually decreased in the x direction, one diameter above and below the source region. This numerical domain allowed an accurate description of the near field, while an excessive refinement in the low-frequency plane-wave propagation region was avoided.

The length of the upstream part of the numerical domain was varied in order to study its influence on the amplitude of the acoustical pressure fluctuations. The length of the upstream block did not have an important effect. This is due to the fact that, as explained above, the cross-junction is an acoustically closed system. A length of two pipe diameters was found sufficient to get computed results independent of this length.

The influence of grid refinement on the results of the numerical simulations was studied by comparing fine, intermediate and coarse-grid results. The fine grid had twice the refinement of the intermediate grid in both x and y directions. In the source region (junction between the main pipe and the closed side branches), the intermediate grid had 40×40 cells and the coarse grid had 30×30 cells. Fig. 14 shows the pulsation amplitudes predicted in terms of the cell width Δx of each grid used for the computations. The number of oscillation periods calculated before reaching a steady oscillation was typically 40.

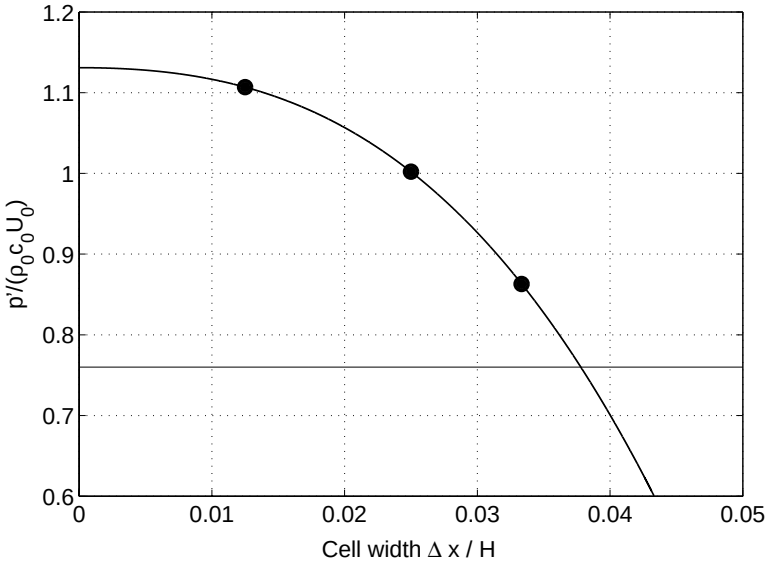

Fig. 14. Pulsation amplitudes $p'/(\rho_0 c_0 U_0)$ numerically predicted for three different cell widths Δx (•). The results are fitted with a polygon of order three of the form: $a + b(\Delta x/H)^2 + c(\Delta x/H)^3$. The experimental value of the pulsation amplitude is also shown (horizontal line). Results obtained for a cross-junction with sharp edges and closed side branches of length $L = 0.564$ m (Strouhal number $S_r = fH/U_0 = 0.27$).

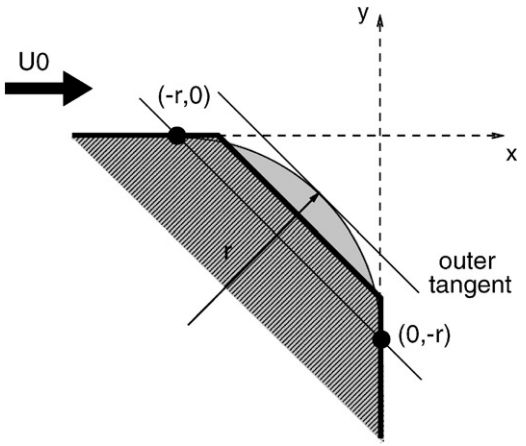

Fig. 15. Size of the chamfer representing a rounded edge.

4.2.4. Kutta condition

Non-linear stability in the numerical method is ensured by means of an additional artificial viscosity term. The magnitude of this dissipation is grid-dependent (decreasing with refinement). However, its presence is sufficient to enforce a Kutta condition near a sharp edge and ensure separation, due to high local cell-to-cell gradients [27]. Therefore, for a cross-junction with sharp edges, separation will automatically occur at the sharp edges. In the case of the cross-junction with rounded edges (Fig. 4), the numerical flow separation is enforced at a fixed point by considering chamfered edges rather than rounded edges (Fig. 15). The chamfer is arbitrarily chosen along the line $[y = -x + r(0.5 - \sqrt{2})]$, half way between the outer tangent and the line joining the points $(-r, 0)$ and $(0, -r)$. Experiments at TU/e have shown that cross-junctions with such chamfered edges have a similar flow behaviour as that observed in cross-junctions with rounded edges [28]. Replacing the rounded edges by chamfered edges changes the pulsation amplitude by less than 10%.

5. Results

5.1. Time dependence of the acoustical pressure

Fig. 16 presents the time dependence of the predicted acoustical pressure at the closed end of a side branch compared to the measured signal for the cross-junction with sharp edges. The dimensionless amplitude $p'/(\rho_0 c_0 U_0)$ shown in Fig. 16 corresponds to the dimensionless amplitude of the acoustical velocity field $|\mathrm{d}\xi/\mathrm{d}t|/U_0$. While the Euler numerical simulations predict the oscillation frequency f within 2%, they overestimate the amplitude of the pulsation amplitudes by 30% (at the Strouhal number considered). This overestimation is partially due to the fact that the numerical method used does not take into account visco-thermal losses. However, calculations by Hofmans [12], based on a vortex-blob method combined with an energy balance including

visco-thermal losses (Section 2.3), also overestimate the pulsation amplitudes by about 30%. This indicates that the discrepancy between theoretical and experimental data could be due to wall vibration effects (Section 2.1). Energy losses in experiments due to wall vibrations are a possible source of the problem and could explain at least 15% discrepancy.

In the case of the cross-junction with rounded edges, very high pulsation amplitudes are reached and shock wave formation was observed both in experiments [2,3] and in our Euler numerical simulations. Fig. 17 shows the history of the acoustical pressure at the end of the closed side branch. The shocks correspond to the local peak in the acoustical pressure at the end wall. The shock wave formation is well predicted by the Euler computations but the amplitude of the

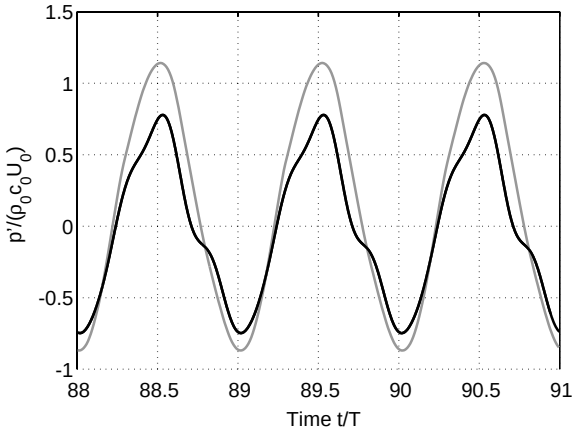

Fig. 16. Cross-junction with sharp edges. Time dependence of the acoustical pressure at the end of a closed side branch. $L = 0.564$ m, $S_r = 0.27$. Experimental data [2] (black line) compared to numerical predictions by means of the Euler code (grey line).

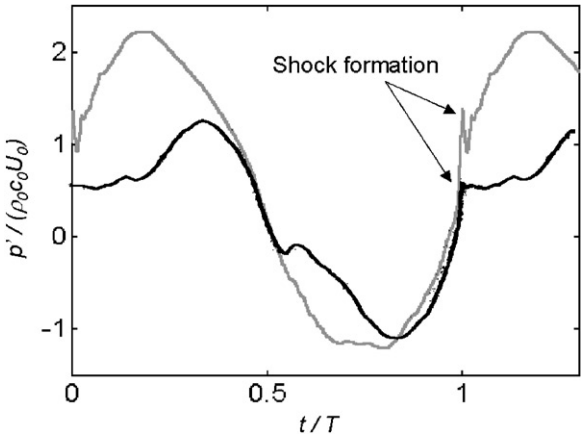

Fig. 17. Cross-junction with rounded edges ($r/H = 0.2$). Time dependence of the acoustical pressure at the end of a closed side branch. $L = 0.476$ m, $S_r = 0.237$. Experimental data [3] (black line) compared to numerical predictions by means of the Euler code (grey line).

pressure oscillations is still 40% higher than the experimental results. Our Euler numerical calculations confirm the conclusion of Hofmans [12] that radiation due to shock wave formation is not sufficient to explain the difference between predicted and observed pulsation levels.

5.2. Flow visualization

Figs. 18 and 19 show the periodic vortex formation in the cross-junction with sharp edges for different times t/T in one period of oscillation T. The predicted magnitude of the vorticity field by means of the Euler computations is compared to the data obtained by Peters [2]. The path of the

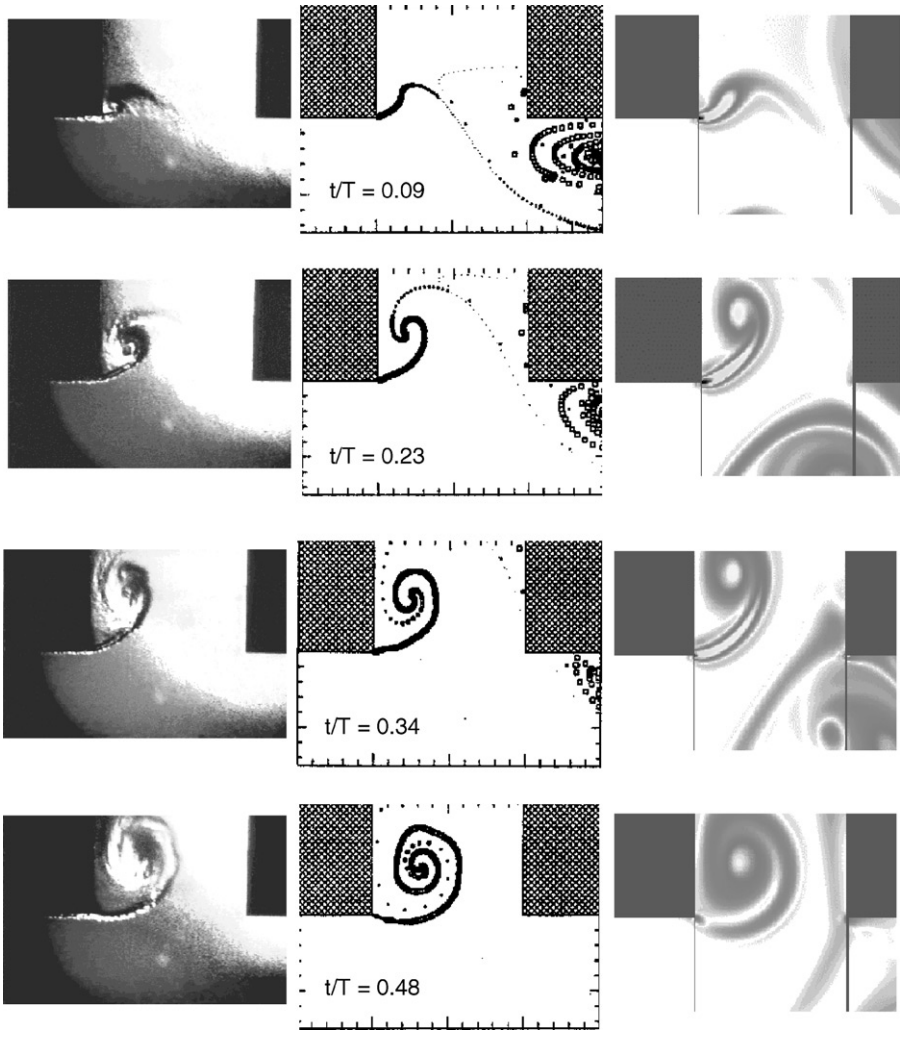

Fig. 18. Periodic vortex formation in the cross-junction with sharp edges ($L = 0.564$ m, $U_0 = 35$ m/s, $f = 156.3$ Hz, $S_r = 0.27$, $(|d\xi/dt|/U_0)_{exp} = 0.76$). Comparison between flow visualization and numerical predictions by means of Peters' vortex-blob method [2] and the Euler calculations (vorticity magnitude). $t/T = 0.09$, 0.23, 0.34 and 0.48 with $t/T = 0$, the point at which the sign of the acoustic velocity becomes positive.

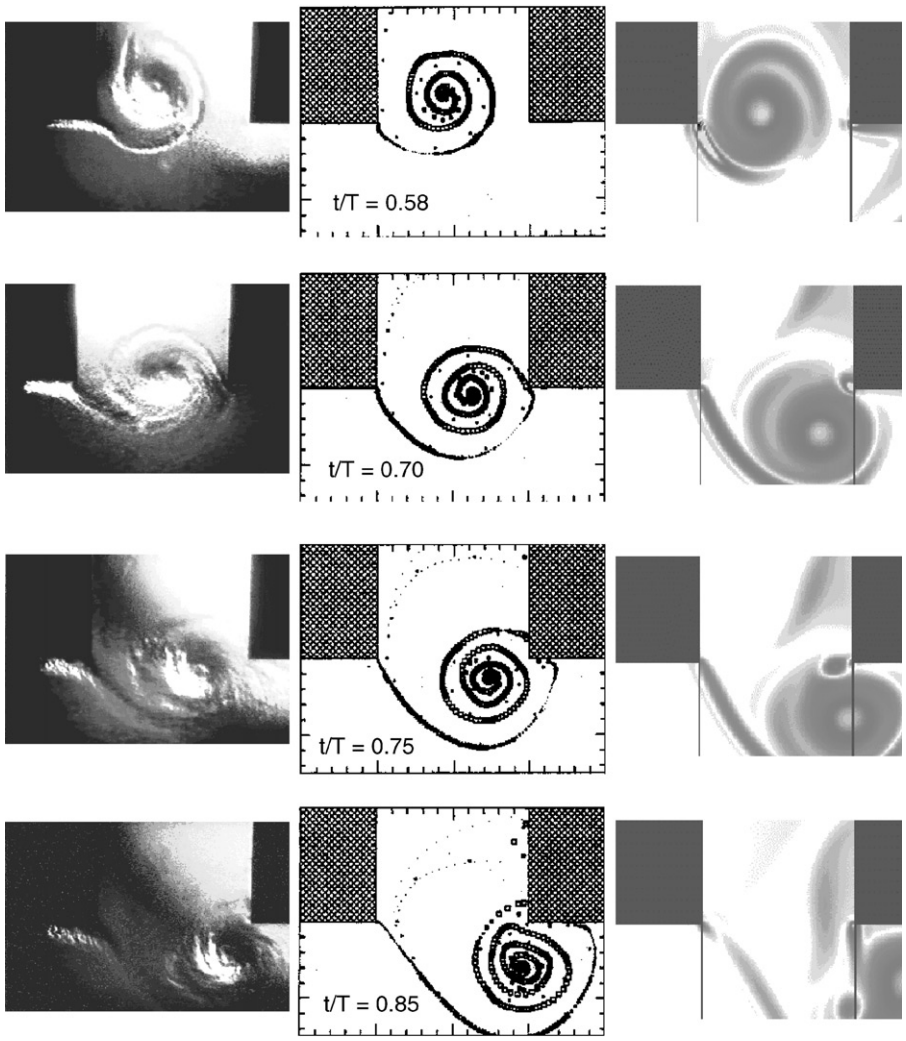

Fig. 19. Periodic vortex formation in the cross-junction with sharp edges ($L = 0.564$ m, $U_0 = 35$ m/s, $f = 156.3$ Hz, $S_r = 0.27$, $(|d\xi/dt|/U_0)_{exp} = 0.76$). Comparison between flow visualization and numerical predictions by means of Peters' vortex-blob method [2] and the Euler calculations (vorticity magnitude). $t/T = 0.58$, 0.70, 0.75 and 0.85 with $t/T = 0$, the point at which the sign of the acoustic velocity becomes positive.

vortex predicted by means of the Peters' vortex-blob method is compared to the path observed in the flow visualization of Peters (Fig. 20). The origin of time is chosen to be the time at which the acoustic velocity field becomes positive (minimum of the pressure in the upper closed side branch). The results shown in Figs. 18 and 19 were obtained for closed side branches with a length $L = 0.564$ m. For this configuration, the pulsation amplitudes were maximal at the critical Strouhal number $S_r = fH/U_0 = 0.27$ (which corresponds to a resonance frequency $f = 156.3$ Hz and a main flow velocity $U_0 = 35$ m/s).

From Figs. 18 and 19, the path of the vortex shed at the upstream edge of the upper side of the junction is deduced. Fig. 20 shows that the vortex path predicted by Peters [2] using the blob

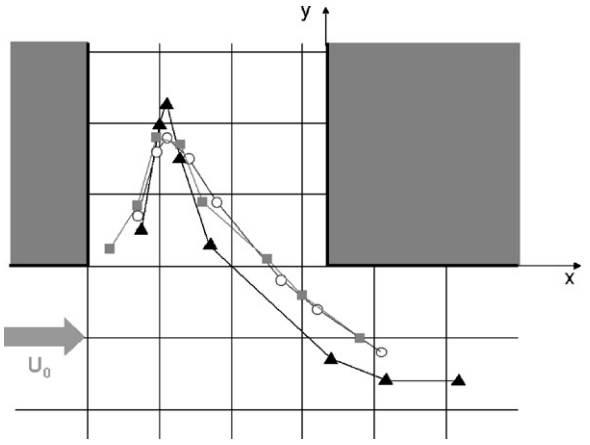

Fig. 20. Vortex path in the cross-junction with sharp edges ($L = 0.564$ m, $U_0 = 35$ m/s, $f = 156.3$ Hz, $S_r = 0.27$, $(|d\xi/dt|/U_0)_{exp} = 0.76$). The data are deduced visually from the pictures shown in Figs. 18 and 19. Comparison between flow visualization (▩) and numerical predictions by means of Peters' vortex-blob method (◦) [2] and the Euler calculations (▲).

method is very close to the experimental vortex path. In these calculations, however, the acoustical amplitude is not predicted but rather imposed as a boundary condition to the incompressible flow simulations of the flow at the junction. The vortex path predicted by the Euler simulations deviates slightly from the experimental results. This is expected to be due to the fact that the theory overestimates the pulsation amplitude by about 30% (Fig. 16). In all cases, the vortex does not hit the downstream edge. Note that our calculations show a significant vortex shedding at the downstream edge of the junction between the side branch and the main pipe (Fig. 19). This vortex shedding is difficult to observe in the flow visualization but does occur. It was ignored in the blob method. Vortex-blob simulations by Hofmans [12] on a similar configuration showed that this vortex shedding at the downstream edge had only a minor effect on the energy balance.

5.3. Dependence on Strouhal number

The amplitude of self-sustained oscillations in a cross-junction depends on the geometry (rounded or sharp edges, length of the closed side branches). The maximum of amplitude occurs at critical Strouhal numbers. The dimensionless amplitude $|d\xi/dt|/U_0$ is shown in Fig. 21 as a function of the Strouhal number $S_r = fH/U_0$. The experimental results are compared with the predicted numerical data obtained by means of our Euler code and with analytical data from the Nelson et al. vortex model for the cross-junctions with either rounded ($r = 0.2H$) or sharp edges.

Again Fig. 21 shows that the amplitudes predicted by the Euler numerical computations are 40% higher than those found in the experiments for the cross-junction with rounded edges (Fig. 21b), and 30% for the cross-junction with sharp edges (Fig. 21a).

In the case of the cross-junction with rounded edges (Fig. 21b), the new analytical model gives a better prediction of the maximum of the amplitude than our Euler numerical calculations.

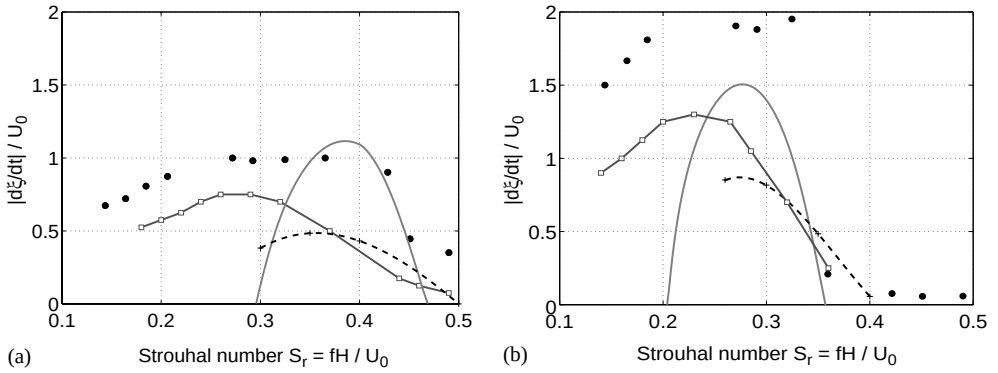

Fig. 21. Dimensionless amplitude $|\mathrm{d}\xi/\mathrm{d}t|/U_0$ as a function of the Strouhal number $S_r = fH/U_0$. (a) Cross-junction with sharp edges, (b) cross-junction with rounded edges ($r/H = 0.2$). The experimental results (□) are compared with analytical data from the Nelson et al. model [7] (——) and from Kriesels' vortex-blob method [14] (– – – – –) and with Euler numerical predictions (●). The length of the closed side branches is $L = 0.61$ m.

Kriesels et al.'s moderate-amplitude approach [14] systematically underestimates the amplitude by a factor of two. The Strouhal number range within which pulsations do occur is much better predicted by the Euler numerical model than by the analytical model and Kriesels et al.'s moderate-amplitude model [14].

6. Conclusions

Self-sustained oscillations at cross-junctions in pipes with square cross-section have been considered. The junction has either sharp or rounded edges. The coupling between acoustic standing waves and instabilities of the shear layers induces self-sustained oscillations. The pulsation amplitudes can reach very large values ($u'/U_0 = O(1)$). The presence of shock waves, visualized by Peters [2] in the cross-junction with rounded edges for low main flow velocities ($M = U_0/c_0 \approx 0.1$), has been confirmed by the present Euler numerical simulations (Fig. 17).

An analytical aero-acoustical model based on Nelson et al.'s vortex model [7] has been proposed. The two resolution methods considered, an energy balance and an averaging method [23], gave almost identical results for the pulsation amplitude (Fig. 12).

The Euler numerical simulations provide a prediction of the measured pulsation amplitudes within 40% (Fig. 21) and predict the oscillation frequency within 2% (Fig. 16). Compared to the analytical model proposed, the Euler numerical simulations provide a much better insight into the flow behaviour in the cross-junctions. Due to the overestimation of the amplitude of the acoustical pressure at the end of a closed side branch, the vortex path predicted by the numerical simulations deviates from the experimental vortex path (Fig. 20). The overestimation of the amplitude of the acoustical pressure at the end of the closed side branches (in our results from the Euler numerical simulations) cannot be explained by the absence of visco-thermal losses alone in the numerical method. Previous calculations by Hofmans [12] for a similar pipe system, based on a vortex-blob method including visco-thermal losses, also overestimated the pulsation amplitudes by 30%. Our

numerical simulations confirm the results of Hofmans [12] showing that radiation losses generated by non-linear wave steepening cannot explain this discrepancy. The difference in predicted and measured pulsation amplitudes could be due to experimental problems such as wall vibrations (Section 2.1). Further research should be carried out to include visco-thermal losses at the wall in an Euler calculation. This could be done by using locally reacting impedance boundary conditions instead of hard wall boundary conditions.

The analytical model based on Nelson et al.'s vortex model is quite attractive for engineering applications. Some research could be carried out to improve its prediction of the Strouhal number range at which pulsations occur.

As an alternative to the analytical model based on Nelson et al.'s vortex model [7], the use of Kriesels et al.'s moderate-amplitude model [14] was considered. In the present case, Nelson et al.'s vortex model seems better because it predicts more accurately the maximum of the pulsation amplitudes (Fig. 21).

Appendix

The conformal mapping is based on the Schwarz–Christoffel transformation [29] of the boundaries of a polygon (in the z-plane) into the real axis of the complex ζ-plane (Fig. 10).

The transformation is given by the relation

$$\frac{\mathrm{d}z}{\mathrm{d}\zeta} = k_1 \zeta^{-1} (\zeta + 1)^{\frac{1}{2}}, \tag{A.1}$$

where k_1 is an arbitrary constant which may be complex.

By integration

$$z = \frac{\mathrm{i}H}{\pi} [2\sqrt{\zeta + 1} + \log(\sqrt{\zeta + 1} - 1) - \log(\sqrt{\zeta + 1} + 1)] + H. \tag{A.2}$$

The complex potential of a point source (at $\zeta = 0$) is

$$\varphi = -\frac{Q_V}{\pi} \log \zeta = \Phi + \mathrm{i}\Psi, \tag{A.3}$$

where Q_V is the rate of emission of volume per unit time. Q_V is related to the acoustical velocity $|\mathrm{d}\xi/\mathrm{d}t|$ and the width H of the pipe:

$$Q_V = \mathrm{i} \left| \frac{\mathrm{d}\xi}{\mathrm{d}t} \right| H. \tag{A.4}$$

Φ and Ψ are the velocity potential and the stream function of the irrotational two-dimensional motion.

The complex acoustical velocity is $u'^* = -\mathrm{d}\varphi/\mathrm{d}z$.

This yields

$$\kappa_n(t) = \frac{u'_y}{\mathrm{d}\xi/\mathrm{d}t} = \left| \frac{1}{\sqrt{\zeta + 1}} \right|. \tag{A.5}$$

The determination of $\kappa_n(t)$ involves the numerical solution of non-linear equations. An analytical solution based on a fit of the numerical solution is proposed. Near the edge ($\zeta = -1, z = 0$), it is known the flow singularity behaves as $z^{-1/3}$ [30]. Therefore the solution is fitted in order to get an analytical expression for $\kappa_n(z)$ in the form

$$\kappa_n(z) = az^{-1/3} + b, \tag{A.6}$$

where $a = 0.1941$ and $b = 0.2978$. In order to check the accuracy of this expression, the integral can be calculated

$$\frac{1}{H}\int_0^H \kappa_n(z)\,\mathrm{d}z = \frac{3}{2}aH^{-1/3} + b = 1.0415 \approx 1. \tag{A.7}$$

As it is assumed that the vortices are convected at the constant velocity U_Γ, the geometric parameter κ_n is then

$$\kappa_n(t) = aU_\Gamma^{-1/3}(t - t_n)^{-1/3} + b. \tag{A.8}$$

References

[1] J.C. Bruggeman, A. Hirschberg, M.E.H. van Dongen, A.P.J. Wijnands, J. Gorter, Flow induced pulsations in gas transport systems: analysis of the influence of closed side branches, Journal of Fluids Engineering 111 (1989) 484–491.

[2] M.C.A.M. Peters, Aeroacoustic Sources in Internal Flows, Ph.D. Thesis, Technische Universiteit Eindhoven, 1993.

[3] P.C. Kriesels, M.C.A.M. Peters, A. Hirschberg, A.P.J. Wijnands, A. Iafrati, G. Riccardi, R. Piva, J.C. Bruggeman, High amplitude vortex-induced pulsations in a gas transport system, Journal of Sound and Vibration 184 (1995) 343–368.

[4] S. Ziada, E.T. Buhlman, Self-excited resonances of two side branches in close proximity, Journal of Fluids and Structures 6 (1992) 583–601.

[5] S.A. Elder, The mechanisms of sound production in organ pipes and cavity resonators, Journal of the Acoustical Society of Japan (E) 13 (1992) 11–23.

[6] M.S. Howe, Acoustics of Fluid-structure Interactions, Cambridge University Press, Cambridge, 1998.

[7] P.A. Nelson, N.A. Halliwell, P.E. Doak, Fluid dynamics of a flow excited resonance. Part II: flow acoustic interaction, Journal of Sound and Vibration 91 (1983) 375–402.

[8] S.J. Hulshoff, A. Hirschberg, G.C.J. Hofmans, Sound production of vortex-nozzle interactions, Journal of Fluid Mechanics 439 (2001) 335–352.

[9] S.J. Hulshoff, EIA: an Euler code for internal aeroacoustics. Part 1: Method Description and User's Guide, Technical Report, Eindhoven University of Technology, Nl, 2000.

[10] S. Dequand, S.J. Hulshoff, H. van Kuijk, J. Willems, A. Hirschberg, Self-sustained oscillations in a Helmholtz-like resonator, Part 2: detailed flow measurements and numerical simulations, in: 7th AIAA/CEAS Aeroacoustics Conference, Maastricht, The Netherlands, May, American Institute of Aeronautics and Astronautics Journal (2001), submitted.

[11] S. Dequand, Duct Aeroacoustics: from Technological Applications to the Flute, Ph.D. Thesis, Technische Universiteit Eindhoven (Nl) & Université du Maine (Fr), 2001.

[12] G.C.J. Hofmans, Vortex Sound in Confined Flows, Ph.D. Thesis, Technische Universiteit Eindhoven, 1998.

[13] R. Krasny, A study of singularity formation in a vortex sheet by the point vortex method, Journal of Fluid Mechanics 167 (1986) 65–93.

[14] P.C. Kriesels, G.C.J. Hofmans, M.C.A.M. Peters, A. Hirschberg, Flow induced pulsation in pipe systems, in: P.W. Bearman (Ed.), Proceedings Sixth International Conference on Flow-induced Vibration, London, 1995, pp. 505–514.

[15] W. Slayton, private communication, 2002.
[16] J.C. Bruggeman, The propagation of low-frequency sound in a two-dimensional duct system with T-joints and right angle bends: theory and experiments, Journal of the Acoustical Society of America 82 (3) (1987) 1045–1051.
[17] A. Hirschberg, Self-sustained aeroacoustical oscillations in gas transport systems: a prediction method for pulsations induced by closed pipe segments, Technical Report, Technische Universiteit Eindhoven, Gasdynamics Group, Laboratory for Fluid Dynamics, Report R-1428-D, 1997.
[18] A. Powell, Theory of vortex sound, Journal of Acoustical Society of America 36 (1) (1964) 177–195.
[19] M.S. Howe, On the absorption of sound by turbulence and other hydrodynamic flows, IMA, Journal of Applied Mathematics 32 (1985) 187–209.
[20] S.W. Rienstra, A. Hirschberg, An Introduction to Acoustics, Technical Report, Eindhoven University of Technology, The Netherlands, May 2001.
[21] A.D. Pierce, Acoustics: An Introduction to Its Physical Principles and Applications, Acoustical Society of America Edition, Acoustical Society of America, Woodburg, NY, 1989.
[22] A. Hirschberg, J. Kergomard, Aeroacoustics of Wind Instruments in Mechanics of Musical Instruments, in: International Centre for Mechanical Sciences, Courses and lecturers, vol. 35, Springer, Wien, Weinrich editors, 1995, pp. 291–369.
[23] A. Nayfeh, Perturbation Methods, Wiley, New York, 1973.
[24] K.W. Thompson, Time-dependent boundary conditions for hyperbolic systems, Journal of Computational Physics 68 (1987) 1–24.
[25] K.W. Thompson, Time-dependent boundary conditions for hyperbolic systems, Journal of Computational Physics 89 (1990) 439–461.
[26] T.J. Poinsot, S.K. Lele, Boundary conditions for the direct simulation of compressible viscous flows, Journal of Computational Physics 101 (1992) 104–129.
[27] C. Hirsch, Numerical Computation of Internal and External Flow, Vols. 1 and 2, Series in Numerical Methods in Engineering, Wiley-Interscience, Chichester, 1990.
[28] K. Burm, Periodieke Wervelafschudding in Vertakte Luchttransport Leidingen: Invloed van Geometrie en Visualisatie, Technical Report, Internal report R-1131S Fluid Dynamics Laboratory, Dept. of Applied Physics, Eindhoven University of Technology (Nl), 1991.
[29] L.M. Milne-Thomson, Theoretical Hydrodynamics, 5th Edition, MacMillan, London, 1968.
[30] L. Prandtl, O.G. Tietjens, Fundamentals of Hydro- and Aeromechanics, Dover Editions, London, 1934.